IEEE Access
Multidisciplinary | Rapid Review | Open Access Journal

Received April 30, 2020, accepted May 18, 2020, date of publication May 25, 2020, date of current version June 8, 2020.

Digital Object Identifier 10.1109/ACCESS.2020.2996973

Highly Sensitive Microsensor Based on Absorption Spectroscopy: Design Considerations for Optical Receiver

USMAN MASUD[1,2], FATHE JERIBI[3], AHMAD ZEESHAN[4], ALI TAHIR[3], AND MUDASSAR ALI[5,6], (Member, IEEE)

[1]Faculty of Electrical and Electronics Engineering, University of Engineering and Technology, Taxila, Taxila 47050, Pakistan
[2]Department of Electrical Communication Engineering, University of Kassel, 34125 Kassel, Germany
[3]College of Computer Science and Information Technology, Jazan University, Jazan 45142, Saudi Arabia
[4]Department of Mathematics and Statistics, FBAS, International Islamic University, Islamabad, Islamabad 44000, Pakistan
[5]School of Electrical Engineering and Computer Science, National University of Science and Technology, Islamabad 44000, Pakistan
[6]Department of Telecommunication Engineering, University of Engineering and Technology, Taxila, Taxila 47050, Pakistan

Corresponding author: Usman Masud (usmanmasud123@hotmail.com)

This work was supported in part by the German Academic Exchange Service (Deutsche Akademische Austausch Dienst (DAAD)), and in part by the European Union (EU).

ABSTRACT The development of a biomedical sensor involves an extremely sensitive optoelectronics system whose foundations lie on intracavity absoprtion spectroscopy. In order to make it convenient for technical reasons to use this application based utility, we implement dual mode competition. All of the components in this system must be investigated in detail. This work concerns with the design of the optical receiver which is mandatory to understand and analyze the received signal. This has been effectively done by designing an inexpensive system which replaces the existing Agilent based setup. Next, the performance of the system has been investigated by using an important parameter Relative Intensity Noise (RIN). The variation of injection current and temperature and their subsequent effect on RIN has been comprehensively examined. This has been enhanced by an investigation of RIN as subject to the mode positions (values of wavelengths) at which the framework is being operated. Through these considerations, the system's behaviour is understood in a much better way as they lead to an improvement in the sensor's realization with high sensitivity and stability.

INDEX TERMS Semiconductor laser diode, optical receiver, relative intensity noise, cavity optomechanics, biomedical sensor.

I. INTRODUCTION

Using the principles of semiconductor lasers, biomedical sensors can be designed for the detection of specific concentration of gases [1], [2]. We know that the precise determination of trace gases in the air is a pioneering requirement on the measurement technology to improve the quality of diagnosis and treatment. Possible fields of application are developed for this work alongside the sensor to the respiratory gas and pollutant analysis [3], [4]. Often the substance to be tested has concentrations in such a small amount that they can be determined only qualitatively with advanced technical equipment which is quite costly in terms of expense and complexity [5], [6]. Thus the sensitivity of information received from the equipment is extremely important for the physicians because small errors in accuracy can lead to severe damage consequently.

In this work, we have designed a laser based biomedical sensor [8], [20] whose working principle is intra cavity absorption spectroscopy [28]. The goal is to detect trace gases for anaesthesiologists which is vital for every major operation in the medical science. To date, the physicians decide to estimate the amount of the medication using their experience and numerous physical parameters like gender or weight on one hand, or an approximate duration of the sickness of the said patient on the other. It would be much safe and efficient to conduct real-time monitoring of the narcotic in the breath, which is based on the exhalation of propofol. This allows the dose not to adapt during the operation and protects especially the health of patients and reduces costs.

The associate editor coordinating the review of this manuscript and approving it for publication was Yizhang Jiang.

On account of the recent advancements in the framework of semiconductor lasers for long-haul transmission networks, optical sensors have received gigantic research enthusiasm for precise analysis in countless schemes [1], [4], [9]. These have been utilized adequately to improve attributes in anatomical purposes [10], [11]. In this manner, they are specifically valuable for various purposes in organic analysis [11], [12]. Explicit methods in optics empower confocal laser input Tomography that empowers doctors to comprehend the dynamics of their sick persons using portraits and pictures [3], [5]. One of the fundamental system to diagnose has been the parameter of noise in optics which enables multivarious analysis [13]. In other words, an exact extraction of laser noise is highly important as it enables the derivation of reliable information from the setup. Besides, this piece of information helps in understanding the laser's function at a specific moment [13], [14]. This demonstrates intensive comprehension and examination of the relationship between this intensity noise and the electromagnetic components involved in that situation.

An amount of information that has been attained from intensity noise can be utilized in numerous dimensions [2], [15], [16]. In terms of lasers, this information paves ways to fabricate and characterize the functional properties like wavelength modulation of the said device [11], [12], [17], [18]. Likewise, the power sharing phenomenon during mode hopping could be deeply analyzed in the lasers which have the capability to operate in multiple wavelengths (multimode operation), just like a tunable lasing device [15]. Based on the said properties, the property of intensity noise investigates the laser in detail [13], [19], a fact that can be extrapolated in practical applications of laser based sensors. On account of these reasons, researchers are investigating laser noise through various methods and strategies to enhance the prospects of Relative Intensity Noise (RIN).

This subject is treated in recent work [8], [20], which contains a main idea for an efficient optical sensor. Contrary to the laser to operate in single-mode optical applications, a multimode laser operation is provided for this sensor. Here it is important to highlight that a multimode laser is not only complicated in terms of understanding of the underlying concept, but it also leads to various technical difficulties in terms of its physical setup [21]. We need to comprehend the existence of numerous modes, understand the intense competition between them, and then record their data correspondingly. To obtain this, the conception of multiple modes demands extraordinary simulations that ought be done with very advanced computational machines. This creates the first problem. Next, in order to implement the system with more modes, one needs a setup that is capable of detecting the optical signal, identify mode competition very efficiently, and then extract the relevant information in a minute span of time.

Therefore, these considerations have to be addressed beforehand. The idea identified in [8] is the implementation of two mode setup such that the modes can be set to a stable equilibrium intensity which reacts strongly to changes such as the injection current, the geometry of cavity structure or the temperature. In naive terms, both modes compete with each other, and thrive strong for their existence. From the change in the intensity of the three variables mentioned above, worthwhile information can also be achieved through RIN. This sensor opens up more areas of analysis methods to the physicians which have so far been denied because they do not achieve the sufficient robustness, efficiency and accuracy [4].

To comprehend the idea and explore its vistas, the mode competition has been analyzed under various wavelengths [20]. A view of the modes' intensities with the intensity ratio (difference between the values of the intensity between both modes) yields an average value of the RIN rate to be 0.1895 l/Hz which mirrors the strength of the mode competition under this situation. Further efforts have been made to control the entire mechanism centrally via software schemes, and the results have been very encouraging [23]. This is essential as the purpose would be to deploy the system in a real-time environment in such a way that the physicians can continuously monitor their patients. Thus the results that have been obtained with and without the developed centralized mechanism have been discussed in detail. The existence of both modes in minute time slots is one of the targets that strengthens the stability of the sensor, and work has been in progress to investigate it with the help of a mechanical chopper [24]. The results have supported the hypothesis that strong mode competition leads to intracavity absorption spectroscopy, as both modes strive hard in this connection [25]–[27]. In order to undergo its implementation in the real time, a P300 brain computer interface scheme is being developed with close collaboration with the biomedical consultants in the hospitals [28] that will aid in a real-time perspective once the product is fully functional.

II. EXPERIMENTAL SYSTEM

Investigation of intensity noise is a sensitive procedure because minute variations during the experiment might translate into significant variations in the output values [27], [31], thereby causing tremendous changes in the results. This is the reason that the entire process ought be performed carefully.

Figure 1 shows the setup of our dual mode fibre based laser sensor which is being considered here [8], [23]. It comprises a Semiconductor Optical Amplifier (SOA), two Variable Couplers (VCs), two Fiber Bragg Gratings (FBGs), a loop mirror, a collimator, and isolators. The inline SOA [43], which has 3 dB optical bandwidth of 45 nm (minimum) and typical 20 dB small signal gain at 1550 nm, together with loop mirror and FBG_i, forms an internal cavity, where as loop mirror and FBG_o form an outer cavity of the laser. The two FBGs, FBG_i and FBG_o have 0.1% of loss and 3 dB bandwidth of 150 pm at wavelengths $\lambda_1 = 1542.4$ nm and $\lambda_2 = 1542$ nm, respectively. They are mounted on aluminium blocks for temperature control. The VCs [35], whose coupling ratio can be tuned from 0 to 100%, are used to couple out the light in the fibre. Commercially available isolators are used to

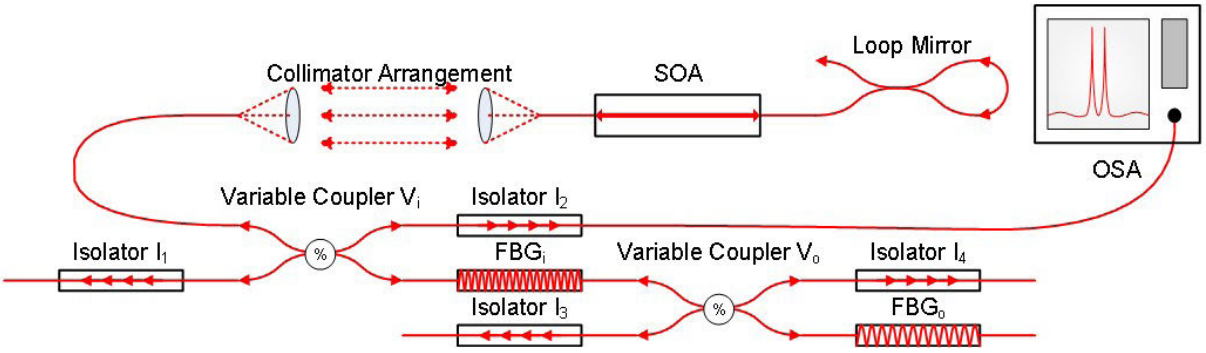

FIGURE 1. Experimental setup of the proposed biomedical sensor [8].

suppress the back reflections in the system, thereby ensuring unidirectional flow of light at the said spots.

An FBG is an optical filter which has stop band centred at Bragg wavelength $\lambda_B = 2r\psi$, where r is the average mode index and ψ is the grating period. A loop mirror is a reflector which reflects its input entirely when counter propagating light waves experience constructive interference. An optical isolator blocks the reflected light back into the input side. Most of the isolators use polarization effect to achieve this goal [33].

When current is supplied to SOA, a multi-wavelength light output is produced whose peak intensity occurs at a value of 1.55 μm. The Laser Diode Controller (LDC) [43] can regulate the amount of its input parameters (temperature and input current), thereby the intensity of the spectrum varies accordingly.

A part of the SOA's output is divided with the help of the VC_i which controls the desired intensity. In this way, the remaining optical intensity moves to the FBG_i which can filter (throw back) a portion of light. In the same way, a part of optical intensity from FBG_i is governed by VC_o's coupling ratio. At the same level, FBG_o rebounds some optical output in the cavity. Each FBG reflects optical intensity according to the respective grating's set wavelength (temperature controlled configuration, 0°C to 1800°C) [45]. Thus there are mainly two cavities in the setup, corresponding to FBG_i (FBG1) and FBG_o (FBG2), as shown in the figure, which correspond to the existence of two modes M_i (M1) and M_o (M2), respectively. It is clear from the figure that VC_i regulates the intensity of the internal and external cavities, while VC_o regulates only the external cavity. The collimator is used to place the sample holder in it, whose absorption characteristics change the optical intensities of the respective modes. This variation is noticed by detection of the intensity noise, thereby justifying the operation of the biomedical sensor.

In order to measure RIN, the setup in figure 2 has been used. After conversion of optical intensity into electrical intensity via photodiode, the DC (average value of the current output) and AC (Low Noise Amplifier (LNA intensifies its output further) components are bifurcated via Bias Tee. Further technical details are provided in [46], [49].

The intensity variations in the sensor can be identified through RIN

$$\mathrm{RIN}(f) = \frac{N(f)}{G_A P_L B}, \tag{1}$$

where, $N(f)$ is laser intensity noise (value after substracting dark noise and shot noise; G_A is the gain of the preamplifier, P_L is the average power detected in the load resistor of the photodiode, and B is the resolution bandwidth of the Electrical Spectrum Analyzer (ESA). Light output is taken from OSA, and a GPIB cable is used for interaction between the devices that helps in regulating the system via LABVIEW (version: 18.0.1) [48].

In this way, the experimentation done is recorded via Digital Multimeter (DMM), Optical Spectrum Analyzer (OSA), and ESA, using GPIB (General Purpose Interface Bus) connection and afterwards digitally saved. We are using LABVIEW (version: 18.0.1) [48] to manipulate this mechanism.

A. DEVELOPMENT OF CONTROL MECHANISM

Considering the design layout of the equipment, the GPIB is used as a connector between computer/controller and instruments. Also called the ANSI/IEEE Standard 488.1−1987 standard [57], it is a parallel data bus with data tranfer rate of 1 Mbyte/s and higher. Therefore, one GPIB hardware can control upto 15 instruments and instruments can be addressed 0 to 30 uniquely [50]. It has capability of encoding the message as ASCII character string using the SCPI (Simple Command Protocol for Instruments) protocol [58].

There are two types of GPIB commands. They are device dependent messages and interface messages. Device dependent messages also called data messages contains device specific information where as interface message also called command messages contains initializing the bus, addressing and unaddressing devices and setting device modes for remote or local programming messages [53].

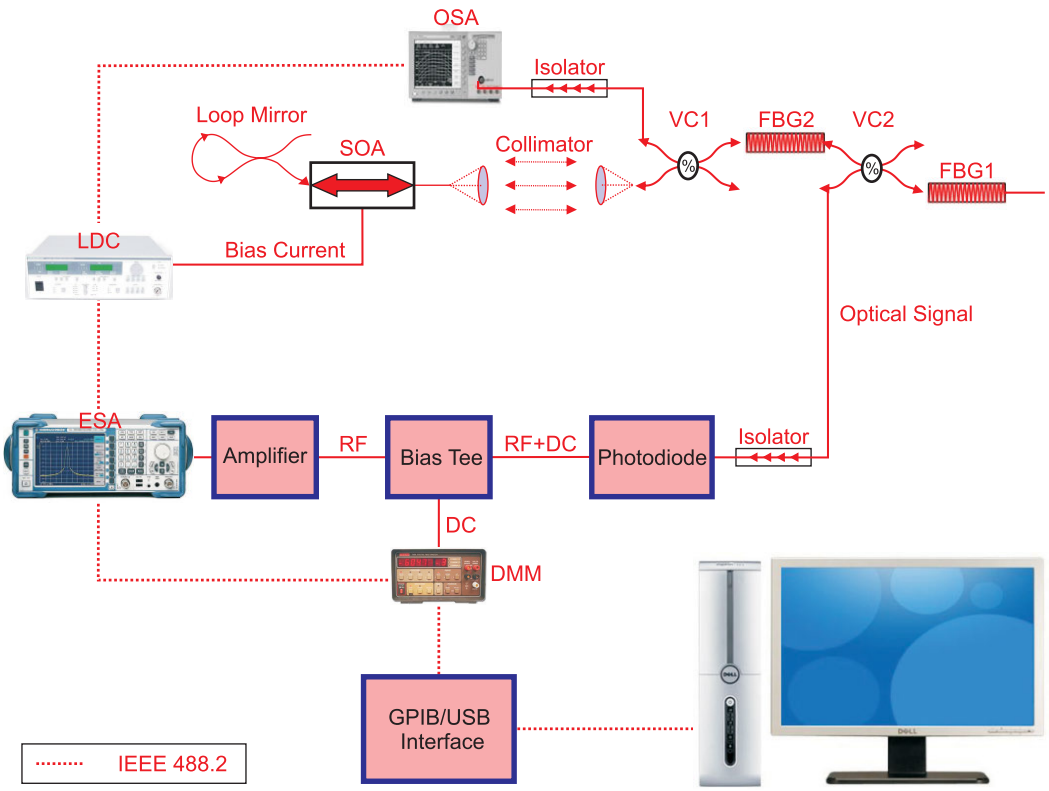

FIGURE 2. Modified experimental system, with amendments in [8].

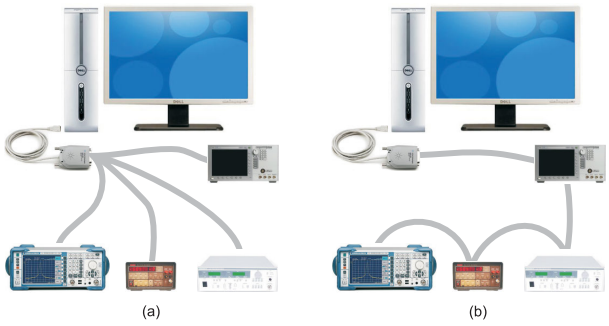

FIGURE 3. Comparison of (a) linear (used in this work), and, (b) star configurations, respectively.

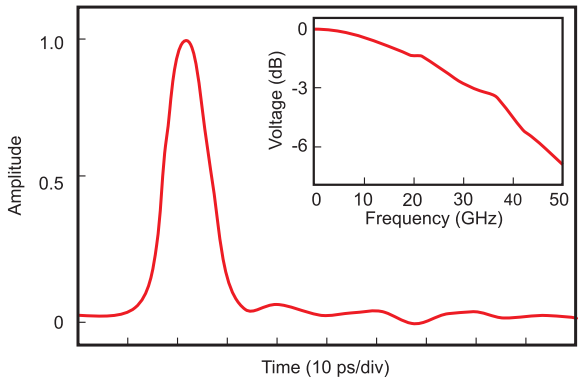

FIGURE 4. Impulse and frequency response of the photodiode [35].

In this way, the GPIB protocol categorizes the devices as talkers, listeners, and controllers. Generally, computer is a controller but simultaneously it can act as a listener and talker too. Controller has to manage the communication link, respond to the devices that request services and pass or take control of the bus. Talker can place the data on the GPIB. Only one instrument at a time can act as a talker in a network. Listener can read data from the GPIB and many devices can act as listener at a same time. Instruments can be connected either using linear configuration, which is used in our work, or star configuration [23], [50], [53]. Both configurations are respectively shown in figure 3.

III. OPTICAL RECEIVER

An optical receiver is a kind of transducer, which converts received optical signal into an electrical signal. Main components of an optical receiver are optical detector and LNA. The combination of an optical detector and LNA, called front end, determines the characteristics of an optical receiver [25], [33], [36].

In our experimental setup, optical receiver has been built by using comercially available PIN photodiode, Bias Tee, and LNA. In this case, determination of an optical receiver characteristic properties become challenging due to correlation of one component's operational parameters with others. This suggests the requirement of analysis of each component, specially photodiode and LNA, from the point of view of their operational parameters. Thus, a short introduction of these components is presented. Also, optical receiver designing

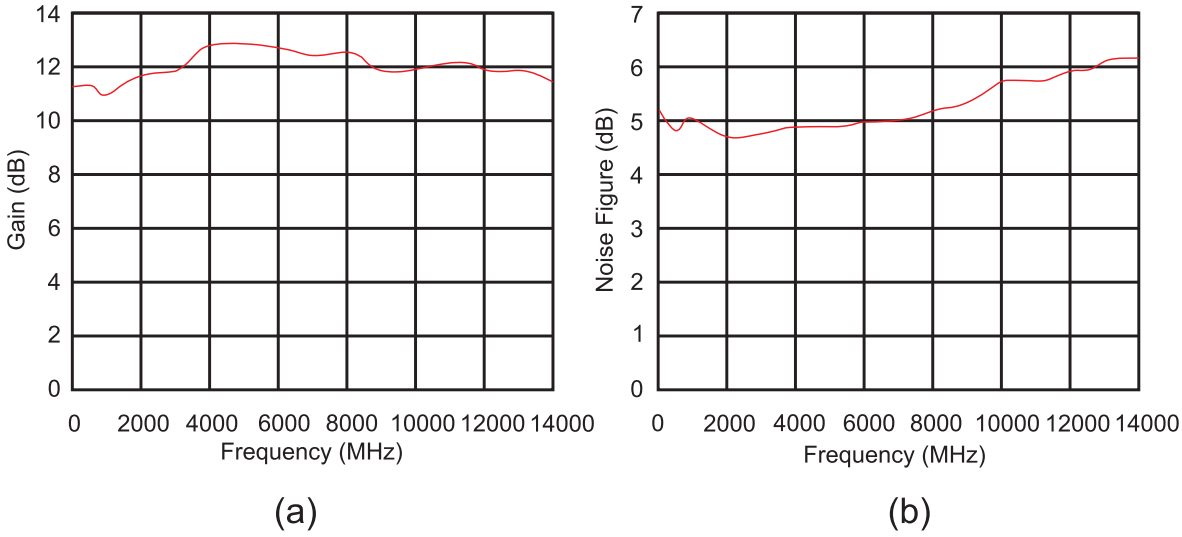

FIGURE 5. Plots of gain and noise figure of the amplifier vs frequency [48].

issues based on the performance parameters are discussed. Furthermore, optical receiver parameters are calculated from the data provided in the manufacturer's catalogue. Finally, the details of the designed optical receiver are presented.

IV. SETUP DETAILS AND OPERATIONAL PRINCIPLE

Based on the discussed design issues which are mandatory for an optical sensor, selection of components is done. We are interested to build an optical receiver for the measurement of laser intensity noise. Thus our design focuses on operating parameters like sensitivity and spectral range of an optical receiver. To design an optical receiver, which has high enough sensitivity so that it can measure intensity noise of laser; high responsivity, low dark current PIN photodiode (Newport: D−15ir) is used. It has typical voltage bandwidth of 29 GHz and is of unamplified type. It has spectral response range from 950−1650 nm, and fiber input connector style FC and output connector type Anritsu-K. Output termination is 1 k.

Figure 4 shows the impulse and frequency response of the photodiode. The output voltage is nearly flat from 0 to 20 GHz and slightly decreases from 20 to 30 GHz. Beyond 30 GHz, the negative slope is high. The useful frequency range of this photodiode is considered from 0 to 30 GHz. More specification detail can be found in [35].

To improve the measurement system noise figure without compromising the system bandwidth, amplifier (Mini-Circuits: ZX60−14012L-S+) is used. It has typical gain of 12 dB and noise figure of 5.5 dB. It has 50 input and output impedance and SMA female connectors (SubMiniature Type A), which are coaxial rf connectors suitable for dc to 18 GHz frequency range, in both input and output terminals. The detailed specification of this device is found in [51].

Figure 5 shows gain and noise figure of the low noise amplifier. They are not flat in required frequency range. Gain and noise figure have typical flatness of ±1 dB. Also, the thermal noise of the optical receiver is a function of the noise figure of the amplifier. Hence, the thermal noise of an optical receiver is not white.

To prevent degradation in DR of an optical receiver, low insertion loss Bias Tee (Mini-Circuits: ZX85−12G−S+) is used. It has connector type SMA female and impedance of 50 in both input and output ports. The detailed specification of the Bias Tee can be found in [52]. During selection of Bias Tee, operating frequency range, type of connectors, input-output impedance, and operating current limit are taken into consideration.

The block diagram of an optical receiver built by using above selected components is shown in figure 6.

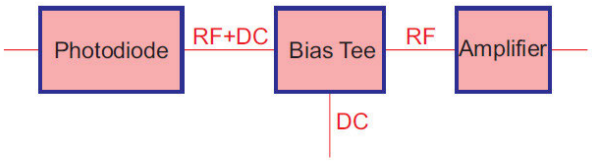

FIGURE 6. Block diagram of an optical receiver.

A. OPERATIONAL PRINCIPLE

The PIN photodiode collect the light from optical sources like laser diode. The electrical signal output from the photodiode contains DC signal as well as AC signal. The DC signal is directly proportional to the average optical power input to the photodiode. The AC signal is the result of addition of noises due to photodiode and laser diode. The Bias Tee, which acts as a filter, splits the DC signal and AC signal. The DC signal can be measured by using digital multimeter of low input impedance. The AC signal, which is very weak, is amplified by LNA.

During amplification, LNA also adds noise to the signal. The amount of this noise is directly proportional to the noise figure of LNA. The amplified noise can be measured by using radio frequency ESA. The magnitude and frequency range

TABLE 1. Calculated parameters of an optical receiver.

Freq. (MHz) $f_L - f_U$	Shot noise @ 1mA (dBm/Hz)	Thermal noise @25°C (dBm/Hz)	Total noise (dBm/Hz)	NEP $pW/\sqrt{Hz}$	Dynamic Range (dB)
0.3-12000	-154.94	-161.83	154.13	28.04	32.13

of signal that can be handled by the built optical receiver, depends upon its DR, sensitivity, and spectral range.

V. SENSITIVITY ANALYSIS AND OPERATING PARAMETERS CALCULATION

The *sensitivity* of an optical receiver is defined as the minimum amount of input power required to perform defined operation correctly [6], [33]. Thus, an optical receiver is said to have high sensitivity, if it requires less amount of input power to perform detection operation. The sensitivity determines operational range in terms of input power, and holds high significance for biomedical applications [2], [36].

A noise equivalent circuit of front end of an optical receiver is shown in figure 7. The signal current generator I_p represents the detected signal, I_{np}, I_{nd}, I_{nb}, I_{nR}, V_{nd}, V_n, and I_n are shot noise due to photocurrent, shot noise due to dark current, shot noise from the background current, thermal noise current, excess noise of the load resistance R_L, detector noise voltage, preamplifier noise voltage, and current noise sources, respectively [6].

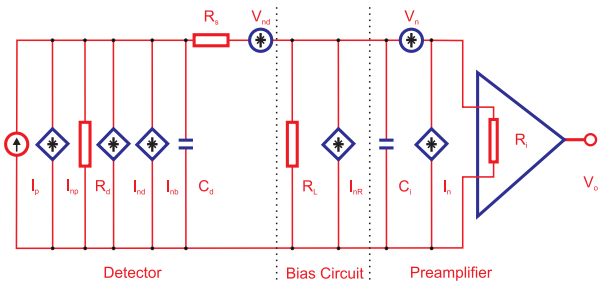

FIGURE 7. Circuit diagram of photodiode-voltage type preamplifier [6].

For simplicity, current and voltage noise sources of the preamplifier are excluded and the preamplifier noise defined only in terms of thermal noise. The SNR of detected signal at the first stage of an optical receiver is calculated as [33]

$$\mathrm{SNR} = \frac{R^2 P_{\mathrm{in}}^2}{2q(RP_{\mathrm{in}} + I_d)\Delta f + 4(k_B T_k / R_L) F_A \Delta f}, \quad (2)$$

where we have used the fact that $I_p = RP_{\mathrm{in}}$. Here, P_{in} is the input optical power to the photodiode. Equation 2 relates the SNR with input optical power. The sensitivity of an optical receiver can be expressed in terms of its Noise Equivalent Power (NEP), which is defined as the minimum optical power per unit bandwidth required to produce (SNR = 1) and is

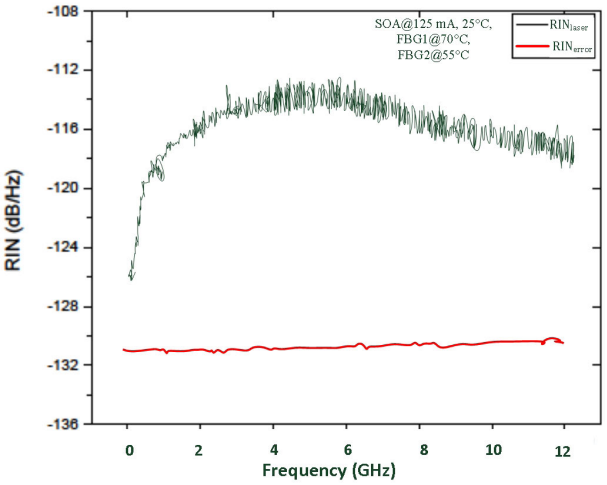

FIGURE 8. Difference between the RIN_{laser} and RIN_{error} when the SOA operates with 125 mA at a temperature of 25°C.

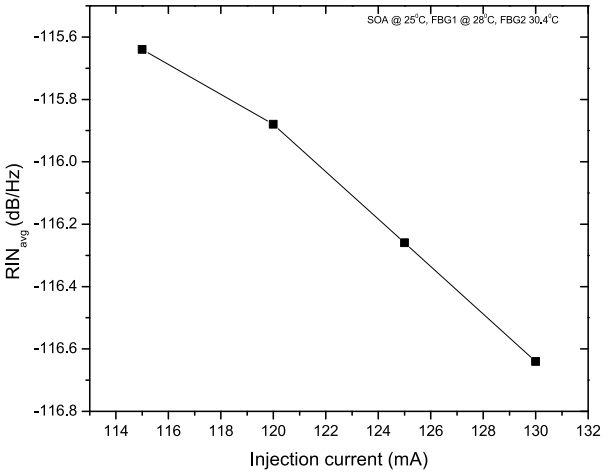

FIGURE 9. Average RIN as a function of injection current when external cavity mode is suppressed. The SOA is set to 25°C.

given by [7], [33]

$$\mathrm{NEP} = \frac{P_{\mathrm{in}}}{\sqrt{\Delta f}} = \frac{[2q(RP_{\mathrm{in}} + I_d) + 4(k_B T / R_L) F_A]^{\frac{1}{2}}}{R}, \quad (3)$$

where $R = \eta q / hf$, η is the quantum efficiency, h is the planck's constant, and f is frequency. The performance of an optical receiver depends on the preamplifier noise sources. Here only the effect due to thermal noise is mentioned, neglecting the parasitic combination of elements of photodiode and preamplifier. Let the maximum input power to the

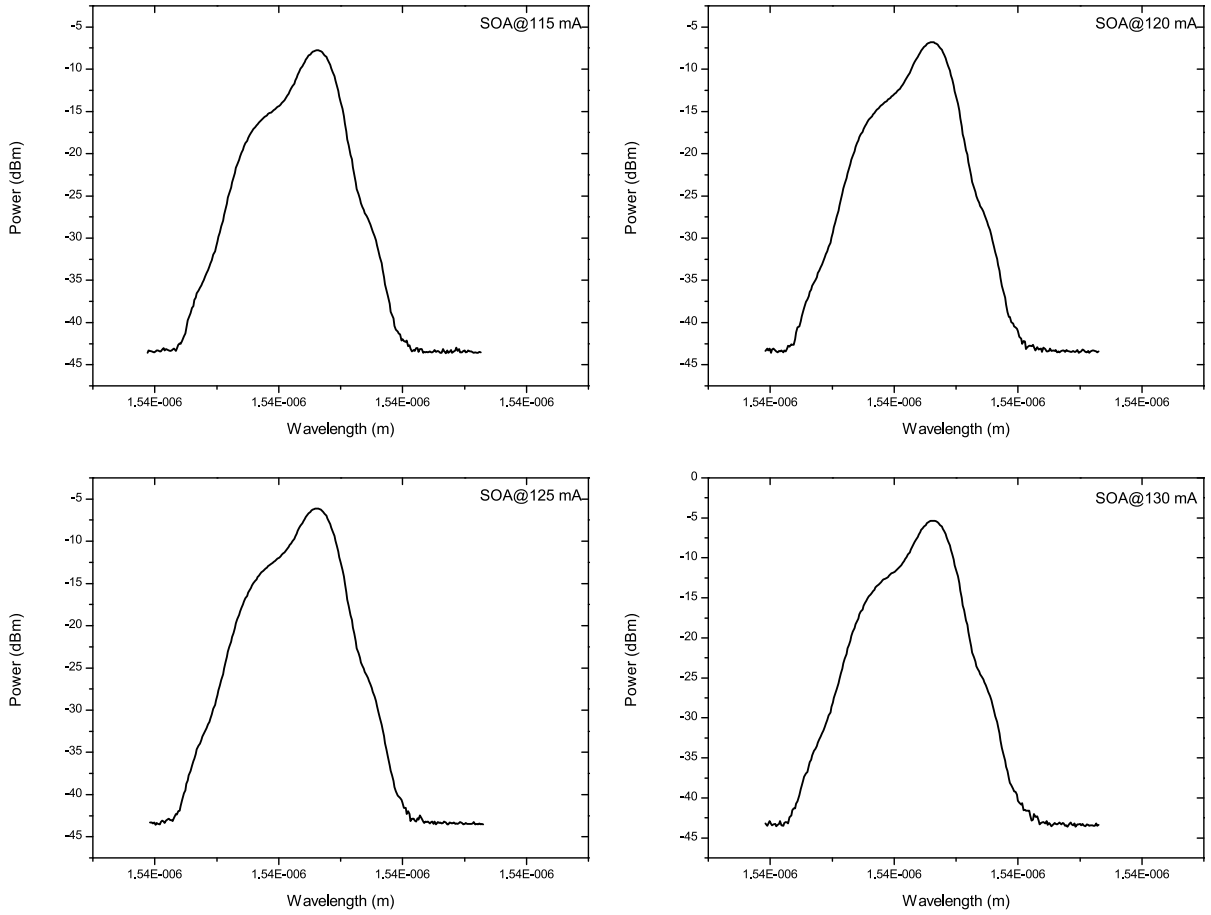

FIGURE 10. Optical view of internal cavity mode at different current when external cavity mode is suppressed.

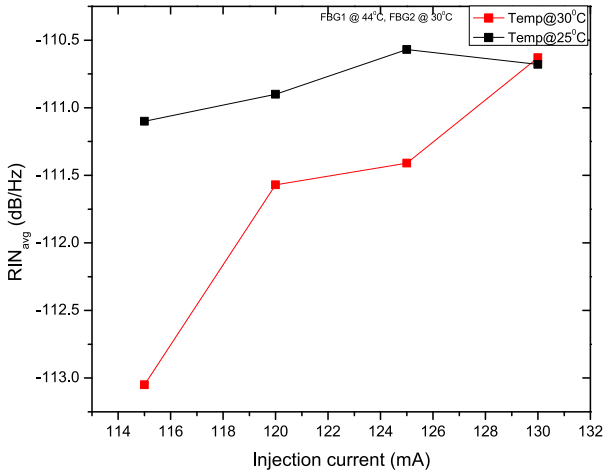

FIGURE 11. Showing effect of increase in temperature and injection current in average RIN.

optical receiver be $P_{\max}$; then the Dynamic Range (DR) can be expressed as [28]

$$\mathrm{DR} = 10 \log \frac{P_{\max}}{\mathrm{NEP}}. \tag{4}$$

The preamplifier has 1 dB compression output of 11 dBm and photodiode has maximum input optical power of 7 dBm, so $P_{\max}$ for eq. 4 equals 7 dBm. Then DR can be calculated using eqs. 3 and 4. Table 1 gives a summary of the optical receiver operating points parameters. All parameters are calculated for average photodiode current I_p of 1 mA at room temperature. The lower limit of operation frequency (f_L) is determined by the amplifier's lower operational frequency and is of 300 KHz frequency. The upper limit (f_U) is determined by the Bias Tee and is of 12 GHz frequency. Shot noise is calculated accordingly for I_p @ 1 mA and I_d @ 20 nA. Dark current of the photodiode is provided in the manufacture's catalogue, from which the thermal noise is calculated. The typical noise figure of 5.5 dB is taken according to the manufacturer's catalogue. The total noise is the sum of calculated thermal noise and shot noise. All noises calculation are normalized to 1 Hz. The NEP, which is the sensitivity of the optical receiver, is calculated according to eq. 3 for responsivity $R = 0.7$ @ 1543 nm. The DR is calculated according to eq. 4 for $P_{\max} = 7$ dBm.

In designing an optical receiver, it has been found that a transimpedance amplifier is suitable to build optical receivers for RIN measurement [23]. This type of amplifier has large

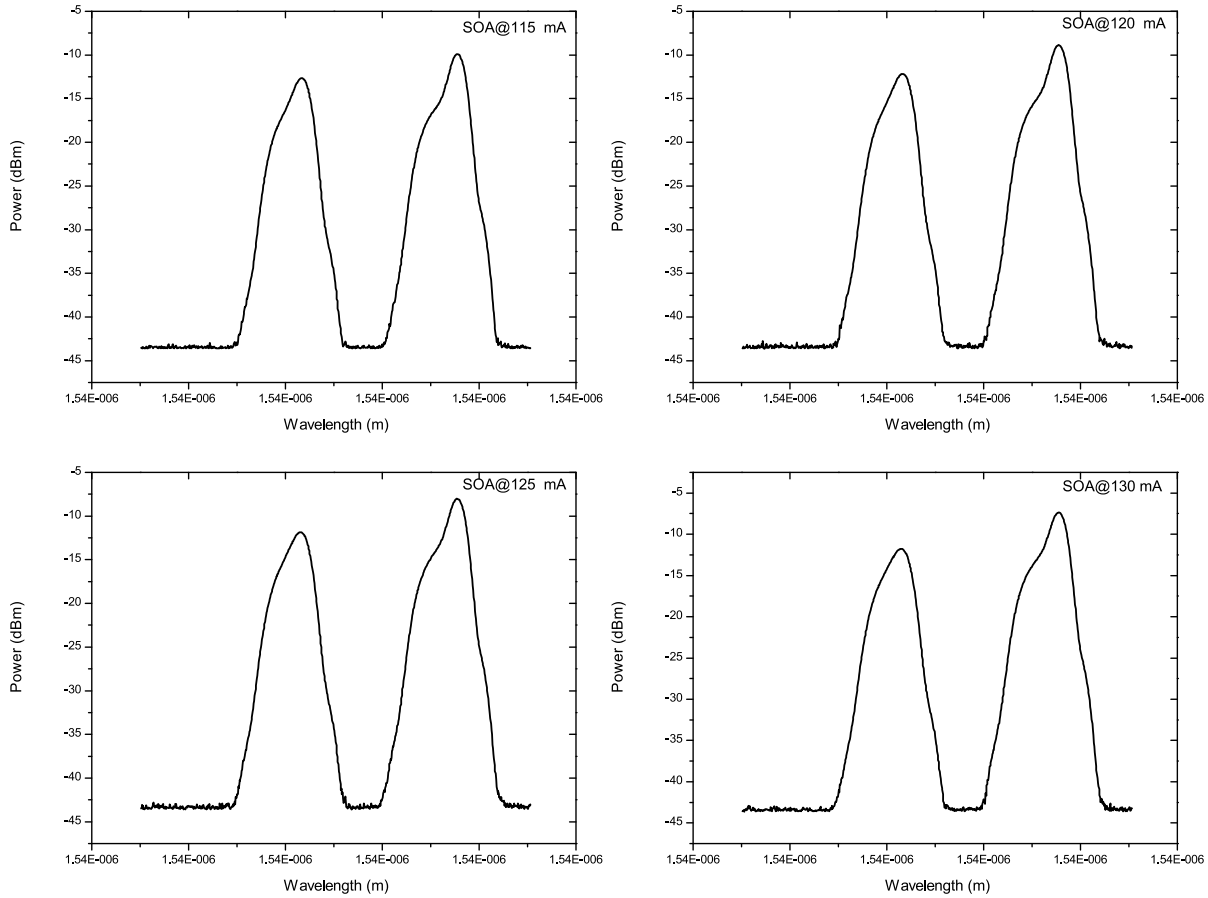

FIGURE 12. Optical view of two modes for SOA @ 25°C.

load resistor but low effective input impedance, hence suitable for the design of high sensitivity large operational bandwidth receiver. Also, amplifier of low noise figure high gain is desired to design large DR optical receiver. The Bias Tee, which is used as a filter to split AC and DC signals, helps to improve the receiver DR by preventing amplifier from saturation. The saturation power of photodiode is less than other components used to built receiver. Hence, DR upper limit of an optical receiver is limited by photodiode.

VI. RESULTS AND DISCUSSION

In order to start the experimentation, it is important to check the restrictions of the measured values of RIN (RIN_{error}) whose intensity should be lower than that of the laser itself (RIN_{laser}). For this, the temperature and injection current of the SOA are kept at 25 °C and 125 mA, respectively. The value of M_i is adjusted to 1542 nm and that of M_o at 1543 nm. In this manner the difference between the wavelengths is 1 nm which yields a contrast of −40.27 dB among both modes along the ordinate. RIN_{laser} has been obtained from 0.1−12 GHz at 650 values of frequency. Afterwards, RIN_{error} has been computed at the same values, using the vendor's specifications [11], [50]. The results have been depicted in figure 8 which shows a difference of 19.32 dB between both average values. RIN_{error} is flat during this wavelength regime at 1.197 dB/Hz (computed at an average photocurrent of 636 μA). This correlation of RIN_{error} and wavelength is because of the devices: both the amplifier and the ESA possess their gain and noise figure which are dependent on the wavelength, as per their respective data sheets and user manuals. On the other hand, the curve is not very flat, making the difference between both values to be −40.27 dB. This indirectly implies a minute impact in recording the RIN from our experimental system. It means that the setup is able to capture RIN with a reasonably high accuracy.

A. RIGHT MODE SUPPRESSION EFFECT IN AVERAGE RIN

The temperature of SOA has been set to 25°C. The internal cavity mode is set to 1542 nm and the external cavity mode is suppressed by adjusting the VC_o.

Measurements are taken from 115 mA to 130 mA bias level with step of 5 mA. Average RIN and corresponding optical spectrum are plotted and shown in figures 9 and 10, respectively in such a manner that the first highlighted point (starting from left of the line) in 9 corresponds to the first graph (top left) in the spectra in fig. 10. In a similar way, the second highlighted point in 9 refers to the second graph (top right) in 10, and so on.

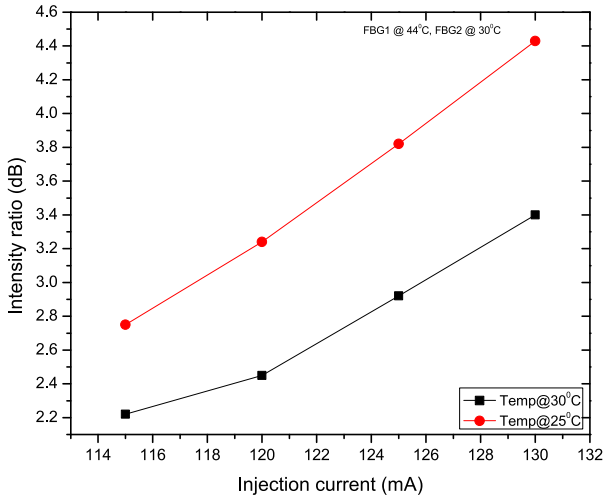

FIGURE 13. Intensity ratio vs injection current.

In figure 9, it is observed that the average RIN decreases with increase in injection current. The theory behind this phenomena can be explained as follows: The increase in injection current decreases the RIN of laser [11], [50], [53]. The relationship between RIN and injection current can be expressed as [50]

$$\text{RIN} \propto \left(\frac{I_{\text{inj}}}{I_{\text{th}}} - 1\right)^{-3}, \tag{5}$$

where, I_{inj} is the injection current and I_{th} is the threshold current. Equation 5 can also be expressed in another way as [11]

$$\text{RIN} \propto P^{-3}, \tag{6}$$

where, P is the output optical signal power. Equations 5 and 6 show the RIN as a function of inverse cube of P. These equations are valid for low bias level, i.e., when a laser is operated near threshold level but when a laser is operated far above the laser threshold level, RIN varies as a function of P^{-3} [11].

Measurements are taken by operating the laser far above the threshold level. Thus, the decrease of only 1 dB in the average RIN is measured for 15 mA difference of bias level.

As a result, the laser diode RIN decreases with increase in injection current and the rate of decrease depends upon its applied level to the diode laser. This experimental result is presented merely to prove that the performance of our diode laser is well described from the adapted theory in physics, i.e., justification of eq. 6.

B. TEMPERATURE AND OPTICAL FEEDBACK EFFECT IN AVERAGE RIN

The intensity noise has been measured for various injection current levels. The experimentation has been performed for the SOA @ 25°C and @ 30°C. The values of M_i and M_o are set to 1542 nm and 1542.5 nm, respectively. Couplers are set fixed during the measurement.

In figure 11, it is observed that the average RIN increases with increase the injection current or output signal power. This is the opposite result then describe by eqs. 5 and 6.

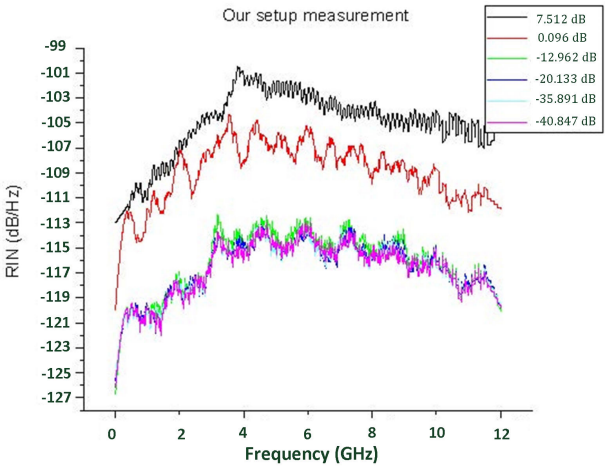

FIGURE 14. Plot of self made RIN setup measurement results for SOA at 125 mA @ 25°C. The values of different intensity ratio M_i/M_o are shown in the enclosed rectangle.

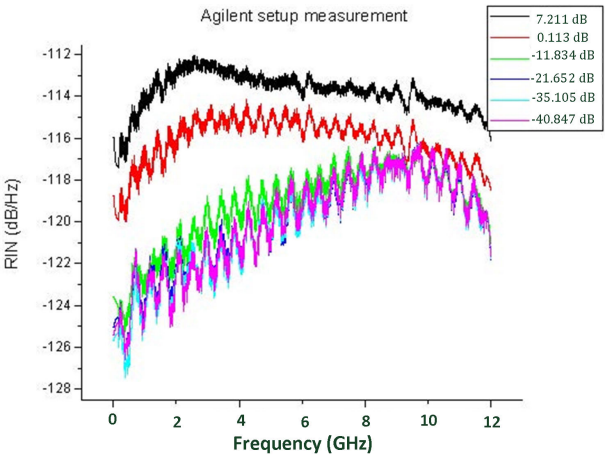

FIGURE 15. Plot of Agilent RIN setup measurement results for SOA at 125 mA @ 25°C. The values of different intensity ratio M_i/M_o are shown in the enclosed rectangle.

Actually, these equations are valid for single mode solitary diode laser. But in this particular operating state, dual mode laser sensor is operated as a single mode laser with external cavity mode as a feedback mode. Hence, the behaviour of our laser in various current levels is very different from ordinary solitary laser diode.

Increase in injection current increases the intensity of the external cavity mode in comparison to the internal cavity mode as shown in figure 12. Although the increment is small, it has large impact on intensity noise and hence on the average RIN of the laser. This results from the fact that the external cavity mode acts as an optical feedback and increase in optical feedback increases RIN [10], [23].

Also in figure 11, it has been observed that the average RIN decreases with increase in temperature. This is because an increase in temperature decreases the gain of semiconductor optical amplifier (SOA) and decrease in gain causes a decrease in amplified spontaneous noise (ASE) [54].

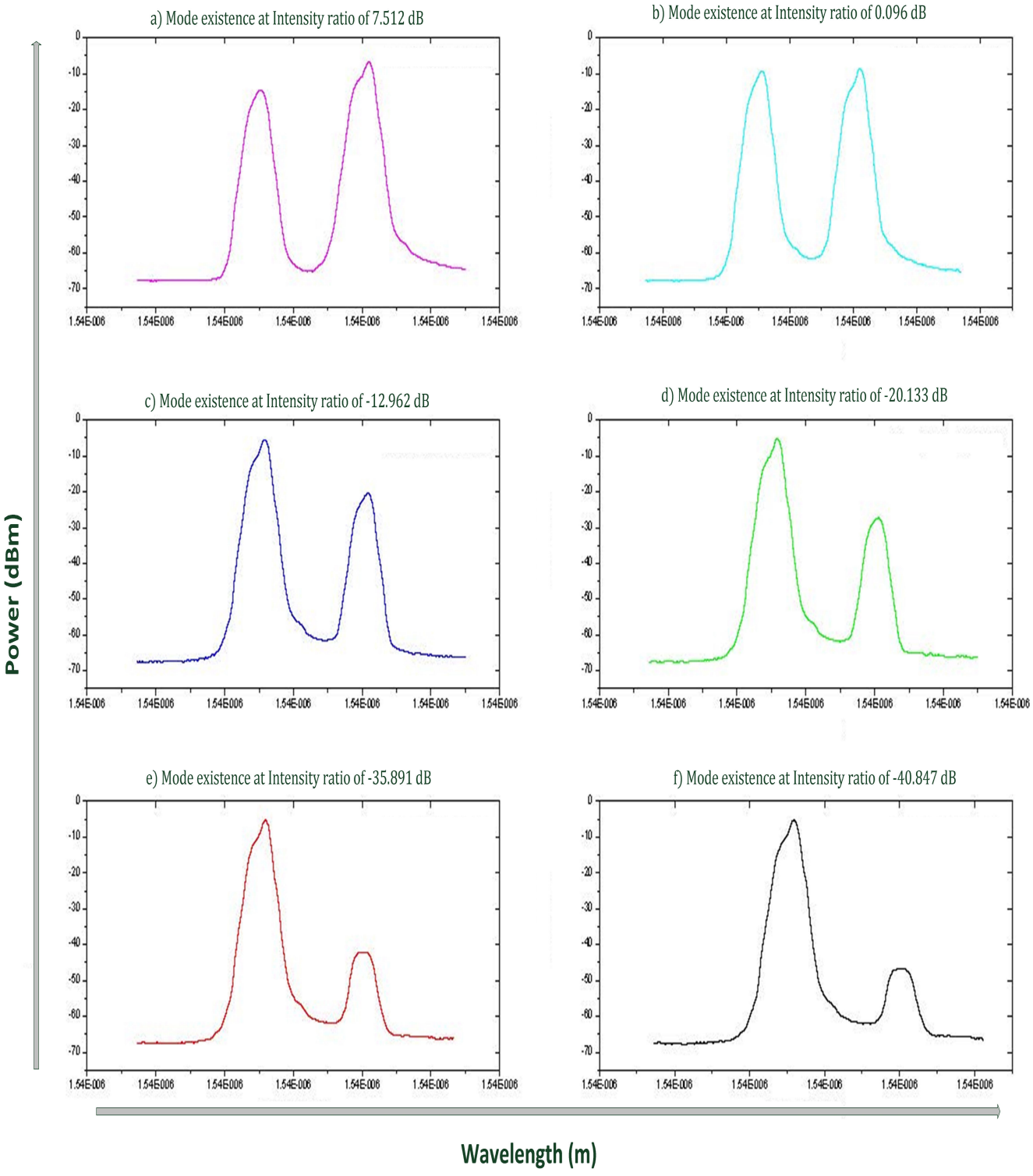

FIGURE 16. Existence of both modes under various conditions.

Furthermore, the noise power spectral density increases slower than gain with the increase in bias current. This effect is more significant at lower temperature. Thus, the slope of the average RIN @ 25°C is smaller than @ 30°C [55], [56].

Comparison based on the relationship between gain, temperature, and ASE does not provide the complete information. Thus, comparing average RIN at both temperatures from the point of view of intensity ratio difference will give

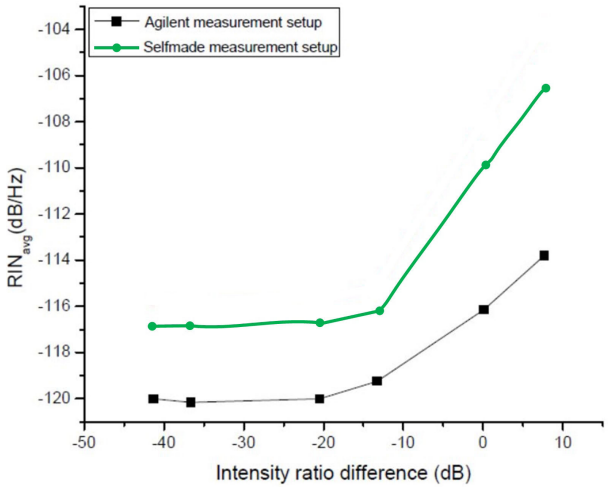

FIGURE 17. Comparing average RIN from both measurement setups.

additional information. In figure 13, intensity ratio of two modes vs injection current for both temperatures are plotted. It is observed that slope and magnitude of intensity ratio difference @ 30°C are smaller than @ 25°C. Also, in figure 11, the average RIN for SOA @ 30°C and 125 mA exceeds the average RIN for SOA @ 25°C and 125 mA. This means, optical feedback has less impact on average RIN in comparison to effect of increase in temperature.

The slope of the average RIN for SOA @ 25°C starts to decrease after 125 mA (this may be the onset of saturation of RIN for this operating condition) but the slope of average RIN for SOA @ 30°C is increasing. This means that the saturation level of RIN at lower temperature reaches earlier than at higher temperature. Thus, from the point of view of sensor, operating laser sensor at higher temperature is good.

Conclusions mentioned above may be valid for only particular operating condition of the laser sensor. From our experiment, we have observed that the RIN not only depends on the modes' intensity ratio difference, but also depends on the injection current and operating temperature. Intensity ratio difference can be made same for different operating conditions by adjusting the VCs. Thus, calculated average RIN and RIN spectrum may be different for same intensity ratio difference of two modes.

C. RIN COMPARISON

With the help of our designed experimental arrangement as well as the Agilent layout, the values of RIN are recorded [20], [52] under equivalent working circumstances. The temperature and current of the SOA is 30°C and 125 mA respectively. Mode M_i is set to 1542 nm and mode M_o is set to 1543 nm. We attempt to equalize this contrast among the intensity ratio to the maximum conceivable value. The corresponding situations appear as shown in figures 14 and 15.

Numerous technical outcomes appear from these plots. First, we consider the system that has been developed in the laboratory in figure 14. It is seen that the pattern of change in the value of RIN seems to be mostly similar for different values of intensity ratios between the inner mode and the outer mode (i.e., the value of M_i/M_o), which are indicated in the enclosed rectangle (from 7.512 to −40.847 dBs). This is important for a biomedical sensor that the behaviour must be consistent along the frequency range of operation, to ensure the precision of results. When this is compared to the Agilent system in figure 15, the trend seems to be a bit different. The intensity ratios of 7.211 and 0.113 dB/Hz are showing a slightly sharp increase and then decrease along the y-axis, shown in the respective figure by black and red colours respectively. For other values of intensity ratio, each value of RIN tends to increase gradually, until it reaches a maximum value at about 10 GHz, and then drops down. To explore the situation in further detail, the relevant situation of both modes under these situations appears in figure 16.

TABLE 2. List of symbols.

F_{A}	noise figure of an amplifier
F_{ESA}	noise figure of an ESA
h	Planck's constant
I	intensity of light
I_{d}	dark current
I_{p}	average photocurrent
P	power; energy flow per unit time
R_L	load resistor
R	responsivity; of photodiode
$S(\omega)$	spectral density
t	instantaneous time
T_k	temperature in kelvin
λ	wavelength of light
λ_{B}	Bragg wavelength
η	efficiency; quantum efficiency
μ	mean of observed data
ω	angular frequency
σ^2	noise variance
δf	frequency bandwidth; of the corresponding device
δI	intensity fluctuation
$\delta\lambda$	wavelength bandwidth
RIN	Relative Intensity Noise
I_{inj}	injection current
I_{th}	threshold current
NEP	Noise Equivalent Power
$N(f)$	laser intensity noise
G_{A}	gain of an amplifier
$\mathrm{VC_i}$/VC1	Variable Coupler corresponding to the inner cavity
$\mathrm{VC_o}$/VC2	Variable Coupler corresponding to the outer cavity
$\mathrm{M_i}$/M1	Mode corresponding to the inner cavity
$\mathrm{M_o}$/M2	Mode corresponding to the outer cavity

With the escalation in optical feedback, the effects are equally observable in each arrangement. This has been elaborated by means of Figure 17 which shows that the value of average RIN varies in both situations. This variation in RIN is analogous to an offset or balance in DC. Likewise, these values of intensity noise at increased frequencies have been similar trends in either setup. Another interesting phenomenon is the variation in Relaxation Oscillation Frequency (ROF) with feedback, which clearly is somewhat opposite for both systems under investigation, i.e., moves ROF towards right along the abscissa (greater frequency) for our system, and vice versa for the Agilent system.

Numerous reasons exist for the distinction in RIN estimation between our arrangement and the Agilent system. We have substituted white noise in place of thermal noise, however it is actually related to the frequency. Besides, facts remain that every gadget in the complete system has an impact on the computation of the outcome values which makes it imperative to calibrate the complete arrangement which is under investigation. Because of these reasons, we have found that the system's performance is reliable. However, we must be careful with the saturation condition of the SOA as any change in the corresponding gain should be considered before utilizing the practicality of the sensor.

Taking these aspects into account, the RIN taken from our arrangement and Agilent arrangement is closely investigated through various perspectives, which involves RIN and its technical impacts on our sensor system. Findings are consistent in the sense that our system in the laboratory can successfully investigate the system's RIN, thereby providing worthwhile technical information.

VII. CONCLUSION

In this work, basic issues related to build a low cost wide spectral range RIN measurement setup have been discussed. It is found that noise added from each measurement system components limits the range of measurement. Thus, a clear understanding of dynamic range of operation is necessary. The uncertainty error of repeated measurement was found high before this work, which indicates the instability of laser setup, and needed to be improved.

A connection has been established and observed between both modes and their corresponding RIN spectra. This analysis extraordinarily helps the utilization of RIN estimations in the region of our spectroscopy based system. Despite changing the spacing (abscissa) between both modes, the value of RIN does not change. In this manner, RIN cannot give knowledge about a distinction of wavelength values among them. A steep inclination of RIN's standard value for higher temperatures indicates an improvement in the performance of our system with hike in temperature. Moreover, it is worth mentioning at this occasion that the system that we have developed in our work is able to obtain the same authentic outcomes which was formerly achievable by the system that used Agilent apparatus. This justifies an inexpensive use of our apparatus for the public as the system is destined for the biomedical sensor.

Sensitivity so as dynamic range of measurement setup can be improved by cascading low noise high dynamic range amplifier. Furthermore, calibration of the measurement setup with the help of poisson laser or ordinary noisy laser with an optical attenuator can be taken as future task to improve measurement results accuracy.

To expand the ongoing analysis, plans to analyze the existence and stability of the modes in minute time intervals are underway, some is recently reported partly in [20]. This is mandatory as the system should have both modes present at all times which is the underlying foundation of the entire concept, while still maintaining the sensitivity of the sensing device.

REFERENCES

[1] Research and Markets. (Mar. 20, 2020). *Gas Sensors Market Analysis 2019-2024-Increased Air Pollution Levels and Need for Air Quality Monitoring in Smart Cities Drives Growth*. [Online]. Available: https://www.prnewswire.com/news-releases/gas-sensors-market-analysis-2019-2024—increased-air-pollution-levels-and-need-for-air-quality-monitoring-in-smart-cities-drives-growth-300995474.html

[2] L. Spinelle, M. Aleixandre, and M. Gerboles, "Protocol of evaluation and calibration of low-cost gas sensors for the monitoring of air pollution," Joint Res. Centre, Ispra, Italy, EUR Sci. Tech. Res. Rep. JRC83791, doi: 10.2788/9916.

[3] X. Luo and J. Yang, "A survey on pollution monitoring using sensor networks in environment protection," *J. Sensors*, vol. 2019, pp. 1–11, Jan. 2019, doi: 10.1155/2019/6271206.

[4] C. Pijolat, C. Pupier, M. Sauvan, G. Tournier, and R. Lalauze, "Gas detection for automotive pollution control," *Sens. Actuators B, Chem.*, vol. 59, nos. 2–3, pp. 195–202, Oct. 1999.

[5] M. D. Foote, P. E. Dennison, A. K. Thorpe, D. R. Thompson, S. Jongaramrungruang, C. Frankenberg, and S. C. Joshi, "Fast and accurate retrieval of methane concentration from imaging spectrometer data using sparsity prior," *IEEE Trans. Geosci. Remote Sens.*, early access, Mar. 12, 2020, doi: 10.1109/TGRS.2020.2976888.

[6] J. P. Dakin and R. G. W. Brown, *Handbook of Optoelectronics*, vol. 1. New York, NY, USA: Taylor & Francis, 2006.

[7] A. Papoulis, *Probability, Random Variables, and Stochastic Processes*. New York, NY, USA: McGraw-Hill, 1991.

[8] U. Masud, *Investigations on Highly Sensitive Optical Semiconductor Laser Based Sensorics for Medical and Environmental Applications: 'The Nanonose'*. Kassel, Germany: Kassel Univ. Press, Jan. 2015.

[9] L. Wang, Y. Li, W. Yue, S. Gao, C. Zhang, and Z. Chen, "High-performance formaldehyde gas sensor based on Cu-doped Sn_3O_4 hierarchical nanoflowers," *IEEE Sensors J.*, early access, Mar. 3, 2020, doi: 10.1109/JSEN.2020.2977972.

[10] K. Petermann, *Laser Diode Modulation and Noise*. Dordrecht, The Netherlands: Kluwer, 1991.

[11] G. P. Agrawal and N. K. Dutta, *Semiconductors Lasers*. New York, NY, USA: Van Nostrand Reinhold, 1993.

[12] F. Effenberger, D. Cleary, O. Haran, G. Kramer, R. D. Li, M. Oron, and T. Pfeiffer, "An introduction to PON technologies," *IEEE Commun. Mag.*, vol. 45, no. 3, pp. S17–S25, Mar. 2007, doi: 10.1109/MCOM.2007.344582.

[13] I. Joindot, "Measurements of relative intensity noise (RIN) in semiconductor lasers," *J. Phys. III*, vol. 2, no. 9, pp. 1591–1603, Sep. 1992.

[14] Z. Zhou, J. Zhang, C. Wang, F. Wan, S. He, and R. Yu, "Non-magnetization detection of arbitrary direction defects in coiled tubing based on fluxgate sensor," *IEEE Sensors J.*, early access, Mar. 9, 2020, doi: 10.1109/JSEN.2020.2979497.

[15] S.-M. Lee, M.-H. Kim, and C.-H. Lee, "Demonstration of a bidirectional 80-km-reach DWDM-PON with 8-Gb/s capacity," *IEEE Photon. Technol. Lett.*, vol. 19, no. 6, pp. 405–407, Mar. 2007, doi: 10.1109/LPT.2007.891978.

[16] E. K. Rotich Kipnoo, D. Kiboi Boiyo, G. M. Isoe, T. V. Chabata, R. R. G. Gamatham, A. W. R. Leitch, and T. B. Gibbon, "Demonstration of Raman-based, dispersion-managed VCSEL technology for fibre-to-the-hut application," *Opt. Fiber Technol.*, vol. 34, pp. 1–5, Mar. 2017, doi: 10.1016/j.yofte.2016.12.001.

[17] G. E. Obarski and J. D. Splett, "Measurement assurance program for the spectral density of relative intensity noise of optical fiber sources near 1550 nm," US Dept. Commerce, NIST, Gaithersburg, MD, USA, Tech. Rep. 250-57, 2000.

[18] V. R. Gonzalez-Diaz and F. Pareschi, "A 65nm continuous-time sigma-delta modulator with limited OTA DC gain compensation," *IEEE Access*, vol. 8, pp. 36464–36475, 2020, doi: 10.1109/ACCESS.2020.2975601.

[19] T. Gensty and W. Elsasser, "Intensity noise performance of semiconductor lasers," Appl. Note 27, ILX lightwave. Accessed: May 26, 2020. [Online]. Available: https://www.newport.com/medias/sys_master/images/images/h9a/h01/8797050044446/AN27-Intensity-Noise-Performance-of-Semiconductor-Lasers.pdf

[20] U. Masud and M. I. Baig, "Investigation of cavity length and mode spacing effects in dual-mode sensor," *IEEE Sensors J.*, vol. 18, no. 7, pp. 2737–2743, Apr. 2018.

[21] R. Tkach and A. Chraplyvy, "Regimes of feedback effects in 1.5-μm distributed feedback lasers," *J. Lightw. Technol.*, vol. 4, no. 11, pp. 1655–1661, Nov. 1986.

[22] V. M. Baev, T. Latz, and P. E. Toschek, "Laser intracavity absorption spectroscopy," *Appl. Phys. B, Lasers Opt.*, vol. 69, pp. 171–202, Sep. 1999.

[23] U. Masud, M. I. Baig, and A. Zeeshan, "Automatization analysis of the extremely sensitive laser-based dual-mode biomedical sensor," *Lasers Med. Sci.*, Jan. 2020, doi: 10.1007/s10103-019-02945-8.

[24] U. Masud, F. Akram, and M. I. Baig, "Behavioural modeling of an optical chopper for intra cavity absorption spectroscopy," in *Proc. Int. Conf. Comput., Electron. Electr. Eng. (ICE Cube)*, Apr. 2016, pp. 11–12.

[25] A. Vizbaras, I. Simonyte, S. Droz, N. Torcheboeuf, A. Miasojedovas, A. Trinkunas, T. Buciunas, Z. Dambrauskas, A. Gulbinas, D. L. Boiko, and K. Vizbaras, "GaSb swept-wavelength lasers for biomedical sensing applications," *IEEE J. Sel. Topics Quantum Electron.*, vol. 25, no. 6, pp. 1–12, Nov. 2019, doi: 10.1109/JSTQE.2019.2915967.

[26] H.-Y. Chung, W. Liu, Q. Cao, R. Greinert, F. X. Kartner, and G. Chang, "Tunable, ultrafast fiber-laser between 1.15 and 1.35 μm for harmonic generation microscopy in human skin," *IEEE J. Sel. Topics Quantum Electron.*, vol. 25, no. 1, Jan. 2018, Art. no. 6800708, doi: 10.1109/JSTQE.2018.2864193.

[27] A. S. Roy, S. Kim, and S. P. Mudanai, "An improved flicker noise model for circuit simulations," *IEEE Trans. Electron Devices*, vol. 64, no. 4, pp. 1689–1694, Apr. 2017.

[28] U. Masud, M. I. Baig, F. Akram, and T.-S. Kim, "A P300 brain computer interface based intelligent home control system using a random forest classifier," in *Proc. IEEE Symp. Ser. Comput. Intell. (SSCI)*, Nov. 2017, pp. 1–5.

[29] J.-M. Liu, *Photonic Devices*. New York, NY, USA: Cambridge Univ. Press, 2005.

[30] R. Ramaswami, K. Sivarajan, and G. Sasaki, *Optical Networks: A Practical Perspective*, 3rd ed. Amsterdam, The Netherlands: Elsevier, 2009, pp. 192–196.

[31] S. Bhattacherjee and A. Biswas, "Investigation on noise performance of $InAs_xSb_{1-x}$ MOSFETs with compositional variations," *Microsyst. Technol.*, vol. 26, pp. 1133–1140, Sep. 2019, doi: 10.1007/s00542-019-04639-1.

[32] J. Ohtsubo, *Semiconductor Lasers: Stability, Instability and Chaos*. Berlin, Germany: Springer-Verlag, 2013.

[33] G. P. Agrawal, *Fiber Optic Communication Systems*. New York, NY, USA: Wiley, 2002.

[34] H. Packard, "Digital communication analyzer (DCA), measure relative intensity noise (RIN)," Product Note 86100-7, 2008.

[35] (Jun. 6, 2018). *Newport*. [Online]. Available: https://www.newport.com

[36] N. Khodaparastasgarabad, A. Mohebbi, and C. Falamaki, "A novel microfluidic high-throughput resistive pulse sensing device for cells analysis," *Microsyst. Technol.*, vol. 25, pp. 3643–3653, Dec. 2018, doi: 10.1007/s00542-018-4278-3.

[37] A. Sharma, I. B. S. Singh, S. Bhattacharya, and S. Sharma, "Performance comparison of DCF and FBG as dispersion compensation techniques at 100 Gbps over 120 km using SMF," in *Nanoelectronics, Circuits and Communication Systems* (Lecture Notes in Electrical Engineering), vol. 511, V. Nath and J. Mandal, Eds. Singapore: Springer, 2019.

[38] H. Talahashi, K. Oda, H. Toba, and Y. Inoue, "Transmission characteristics of arrayed waveguide N×N wavelength multiplexer," *J. Lightw. Technol.*, vol. 13, no. 3, pp. 447–455, Mar. 1995, doi: 10.1109/50.372441.

[39] C. Bock and J. Prat, "WDM/TDM PON experiments using the AWG free spectral range periodicity to transmit unicast and multicast data," *Opt. Express*, vol. 13, no. 8, pp. 2887–2891, 2005, doi: 10.1364/OPEX.13.002887.

[40] M. Fox, *Quantum Optics An Introduction*. New York, NY, USA: Oxford Univ. Press, 2006.

[41] M. A. Parker, *Physics of Optoelectronics*. New York, NY, USA: Taylor & Francis, 2005.

[42] (Feb. 2016). *ITU-T Recommendations, G-Series, Supplement 39*. Accessed: May 24, 2019. [Online]. Available: https://www.itu.int/ITU-T/recommendations/rec.aspx?id=12840lang=en

[43] (Jan. 11, 2019). *Inphenix: IPSAD1501 Semiconductor Optical Amplifier (SOA)*. [Online]. Available: http://www.inphenix.com/pdfdoc/Application_Notes_for_SOAs.pdf

[44] (Feb. 21, 2019). *ILX Lightwave: LDC 3900 Laser Diode Controller*. [Online]. Available: https://www.newport.com/f/4-channel-modular-laser-diode-controller-ldc-3900

[45] (Feb. 16, 2019). *Eurotherm: 3216 Temperature Controllers*. [Online]. Available: https://www.eurotherm.com/de/products/pid-regler/einkanalregler/3200-temperature-process-controller/

[46] (May 2, 2019). *Rohde & Schwarz: FSP30*. [Online]. Available: https://www.rohde-schwarz.com/us/product/fsp-productstartpage_63493-8043.html

[47] (Apr. 13, 2019). *Agilent: 86142B*. [Online]. Available: https://www.equipland.com/commerce/ccp856-agilent-hp-86142b-86142a-86140a-86140b-optical-sp-86142b-osa16.htm

[48] (Mar. 3, 2019). *LabVIEW 2018 Service Pack 1 Readme for Windows*. [Online]. Available: http://www.ni.com/pdf/manuals/374715k.html#known

[49] U. Masud, M. Ali, and M. Ikram, "Calibration and stability of highly sensitive fibre based laser through relative intensity noise," *Phys. Scripta*, vol. 95, Feb. 2020, Art. no. 055505, doi: 10.1088/1402-4896/ab7540.

[50] *Matthew Otis, GPIB Communication*, Texas A & M Univ., College Station, TX, USA. Accessed: May 26, 2020. [Online]. Available: https://fr.scribd.com/document/401985553/GPIBCommunication-doc

[51] (Jan. 13, 2019). *Mini-Circuits*. [Online]. Available: http://www.minicircuits.com/pdfs/ZX85-12G+.pdf

[52] (Feb. 10, 2019). *Mini-Circuits*. [Online]. Available: http://www.minicircuits.com/pdfs/ZX60-14012L+.pdf

[53] R. Bitter, T. Mohiuddin, and M. Nawrocki, *LabView Advanced Programming Techniques*. Boca Raton, FL, USA: CRC Press, 2007.

[54] M. J. Connelly, *Semiconductor Optical Amplifiers*. Dordrecht, The Netherlands: Kluwer, 2004.

[55] M. Shtaif and G. Eisenstein, "Noise properties of nonlinear semiconductor optical amplifiers," *Opt. Lett.*, vol. 21, no. 22, pp. 1851–1853, 1996.

[56] D. Dahan and G. Eisenstein, "The properties of amplified spontaneous emission noise in saturated fiber Raman amplifiers operating with CW signals," *Opt. Commun.*, vol. 236, nos. 4–6, pp. 279–288, Jun. 2004.

[57] *LabVIEW User Manual*, Nat. Instrum., Austin, TX, USA, Part Number 320999B-01, 1992.

[58] J. Travis and J. Kring, *LabVIEW for Everyone: Graphical Programming Made Easy and Fun*. Upper Saddle River, NJ, USA: Prentice-Hall, 2006.

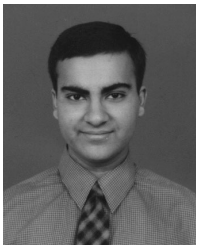

USMAN MASUD received the B.Sc. degree in electrical engineering from the University of Engineering and Technology, Taxila, in 2005, the M.S. degree in electrical engineering in Germany, in 2010, and the Ph.D. degree (by research work), in 2014. His areas of expertise include laser systems, biomedical sensors, spectroscopic applications, and wireless networks. He has been involved in multiple research areas at the moment and finds deep interest in laser-based biomedical applications. He has been an Active Member of Verband der Elektrotechnik, Elektronik und Informationstechnik e.V. (VDE) for several years.

FATHE JERIBI received the B.S. degree in information systems from Jazan University, Jazan, Saudi Arabia, in 2010, the M.S. degree in computer science and information technology from Sacred Heart University, CT, USA, in 2014, and the Ph.D. degree in information technology from Towson University, MD, USA, in 2018. He is currently an Assistant Professor at the College of Computer Science and Information Technology, Jazan University. He has served as an Adjunct Faculty at Towson University, USA, for two years. His areas of interest include networks, databases, software engineering, information and knowledge engineering, and modeling and simulation.

AHMAD ZEESHAN is currently an Associate Professor of mathematics at International Islamic university, Islamabad, Pakistan. He has published more than 100 peer-reviewed articles, mostly in ISI indexed journal. He also published a book: *Analytic Solutions of Non-Linear Partial Differential Equations* (Lambert Academic Press, 2011). He is categorized as highly cited researcher in the year of 2019. His works have been published in journals like *Communications in Nonlinear Science and Numerical Simulation*, *Journal of Magnetism and Magnetic Materials*, *International Journal of Heat and Mass Transfer*, ZAMP, and several other peer-reviewed international journals.

ALI TAHIR received the B.S. degree in computer engineering and the M.S. degree in telecom engineering from the University of Engineering and Technology (UET), Taxila, Pakistan, in 2006 and 2010, respectively. He is currently pursuing the Ph.D. degree in computer science with COMSATS University Islamabad, Wah Campus, Pakistan. He served for Nokia Siemens Network, for two years, as a BSS Engineer. He also served for SCB and AHQ, Islamabad, as a Network Engineer. He is also working as a Lecturer at the College of Computer Science and Information Technology, Jazan University, Saudi Arabia. His areas of interest include wireless networks, distributed systems, software defined networking, network security, and software engineering.

MUDASSAR ALI (Member, IEEE) received the B.S. degree in computer engineering and the M.S. degree in telecom engineering from the University of Engineering and Technology, Taxila, Pakistan, in 2006 and 2010, respectively, with a major in wireless communication, and the Ph.D. degree from the School of Electrical Engineering and Computer Science (SEECS), National University of Sciences and Technology (NUST), Pakistan, in 2017. From 2006 to 2007, he worked as a Network Performance Engineer with Mobilink (An Orascom Telecom Company). From 2008 to 2012, he worked as a Senior Engineer Radio Access Network Optimization with Zong (A China Mobile Company). Since 2012, he has been an Assistant Professor at Telecom Engineering Department, University of Engineering and Technology, Taxila, Pakistan. His research interests include 5G wireless systems, heterogeneous networks, interference coordination, and energy efficiency in 5G green heterogeneous networks.